Supporting information

Polymorphs, Ionic-Cocrystal and Inclusion Complex of N-Amino-1,8-Naphthalimide

Jagajiban Sendh, Jubaraj B. Baruah*

Content List

Figure S23	: Experimental powder XRD patterns of the **$[CuL_2(NO_3)_2]$** (top) and **$[CuL_4](NO_3)_2$** (bottom) complex.
Figure S24	Zeta-potential plots of aqueous solution of (i) **$[HL]NO_3.H_2O$** (1360 µM) salt; (ii) **$[HL]NO_3.L.H_2O$** (330 µM) ionic co-crystal; (iii) **$[CuL_2(NO_3)_2]$** (540 µM) complex; (iv) **$[CuL_4](NO_3)_2$** (225 µM) complex and (v) **$[CdL_3(NO_3)](NO_3).2L$** (257 µM) complex. (vi) L (1 mM aqueous solution). In each case 0.5 ml were taken for the respective measurement.
Figure S26	The excitation and emission spectra of (a) **L**; (b) **$[LH]NO_3.H_2O$** ; (c) **$[LH]NO3.L.H_2O$** ; (d) **$CdL_3(NO_3)](NO_3).2L$** (in each case 3ml solution of 10 mM conc. in methanol, λex = 380 nm in each case).
Table 1S	Hydrogen bond parameters of polymorph, ionic-crystal and metal complexes.

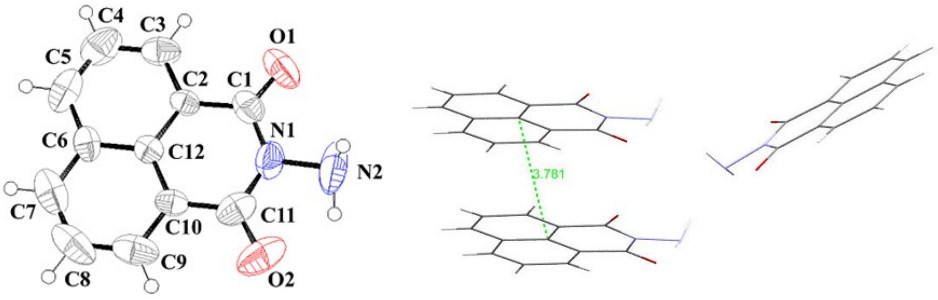

(a) (b)

Figure S1: (a) ORTEP diagram of **L-1 (**thermal ellipsoids drawn with 50% probability); (b) Stacking between the naphthalimide rings of **L-1**.

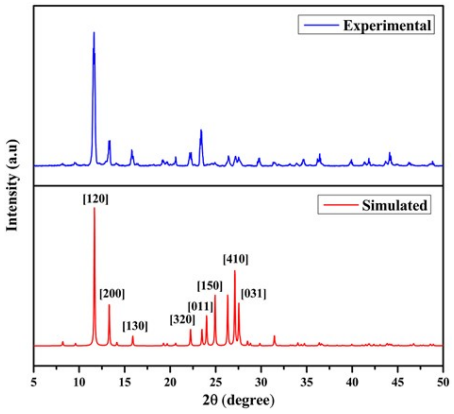

Figure S2: Experimental (top) and simulated (bottom) PXRD patterns of **L-1**.

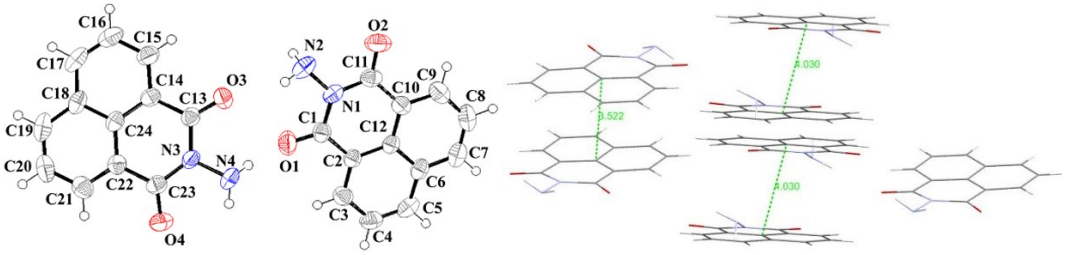

(a) (b)

Figure S3: (a) ORTEP diagram of **L-2 (**thermal ellipsoids drawn with 50% probability); (b) Stacking between the naphthalimide rings of **L-2**.

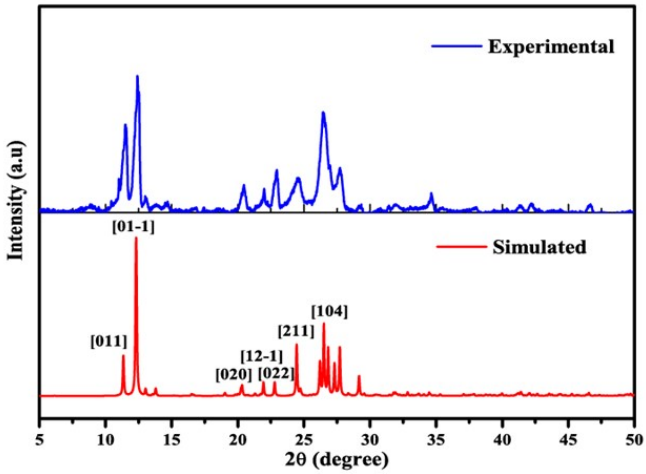

Figure S4: PXRD patterns of **L-2** (top experimental, bottom simulated from CIF file).

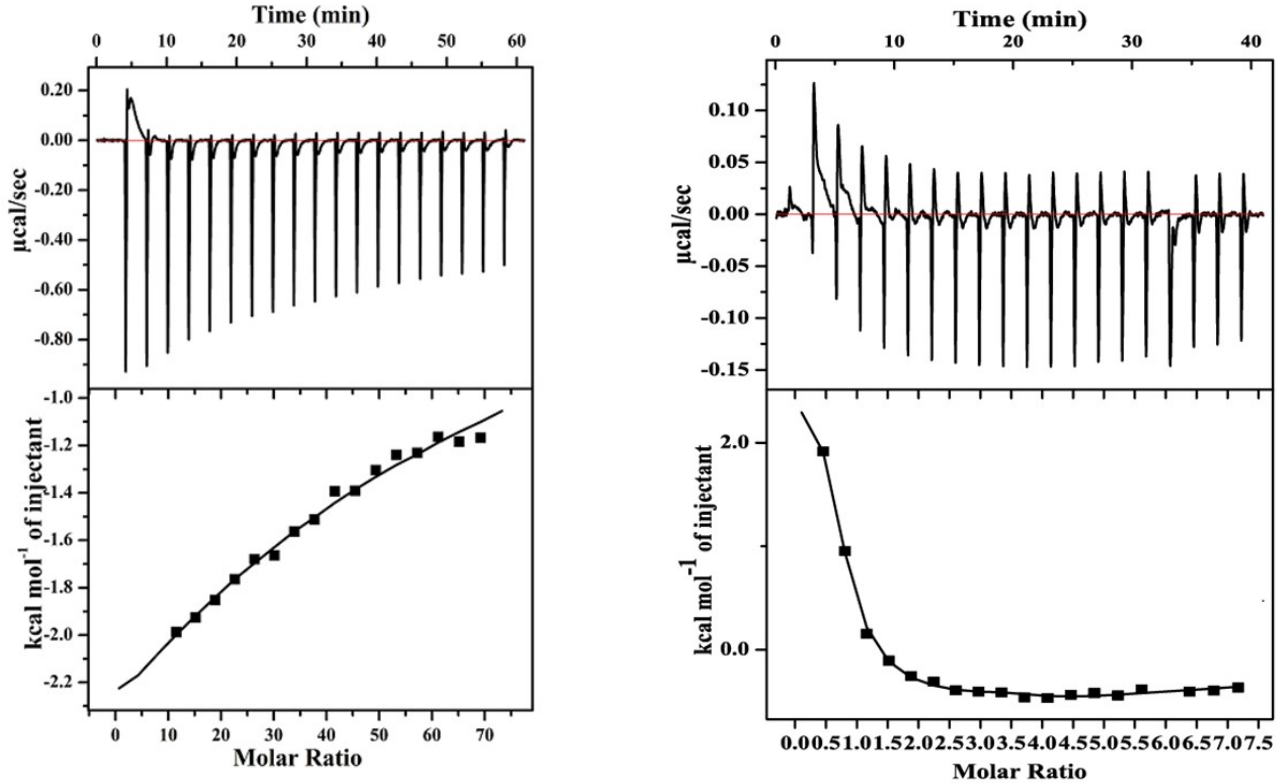

(a) (b)

Figure S5: Isothermal calorimetric titration of compound **L** (5×10^{-6} M) (a) with $Zn(NO_3)_2..6H_2O$ (2.5×10^{-4} M) (each time 2 µL addition for 20 times) in milliQ water; and graph fitted to two sequential equilibrium $K_1 = (3.29 \pm 0.78) \times 10^3$ M^{-1}, $K_2 = (0.71 \pm 0.13) \times 10^3$ M^{-1}, with entropy change for the first equilibrium -439 cal/mol/deg, and -1.14 cal/mol/deg for second equilibrium. (b) Isothermal calorimetric titration of compound **L** (0.02 mM) with $Cu(NO_3)_2.3H_2O$ (1mM) (each time 2µL addition for 20 times) in milliQ water; and graph was fitted to four sequential equilibrium $K_1 = (12.1 \pm 9.6) \times 10^5$ M^{-1}, $K_2 = (3.79 \pm 7.4) \times 10^4$ M^{-1}, $K_3 = (2.43 \pm 4.2) \times 10^6$ M^{-1}, $K_4 = (2.88 \pm 1.7) \times 10^3$ M^{-1} with entropy change for the first equilibrium 35.9 cal/mol/deg, second equilibrium -1.67 cal/mol/deg, third equilibrium 47.0 cal/mol/deg, fourth equilibrium -22.2 cal/mol/deg.

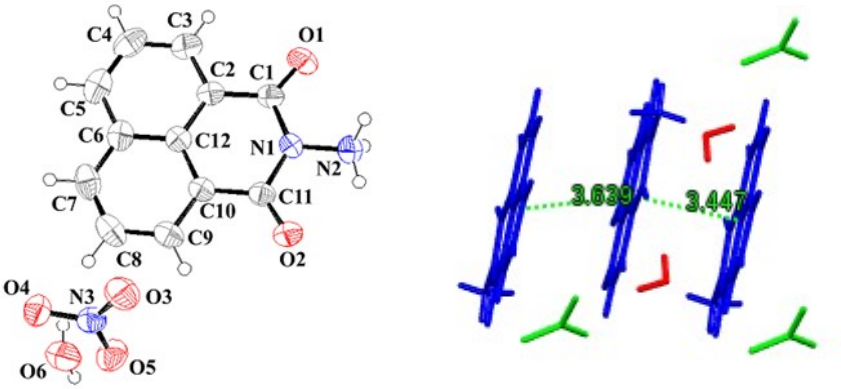

(a) (b)

Figure S6: (a) The structure of **[HL]NO_3.H_2O (**thermal ellipsoids are with 50% probability), (b) stacking among the HL^+ ions (viewed along the c-axis).

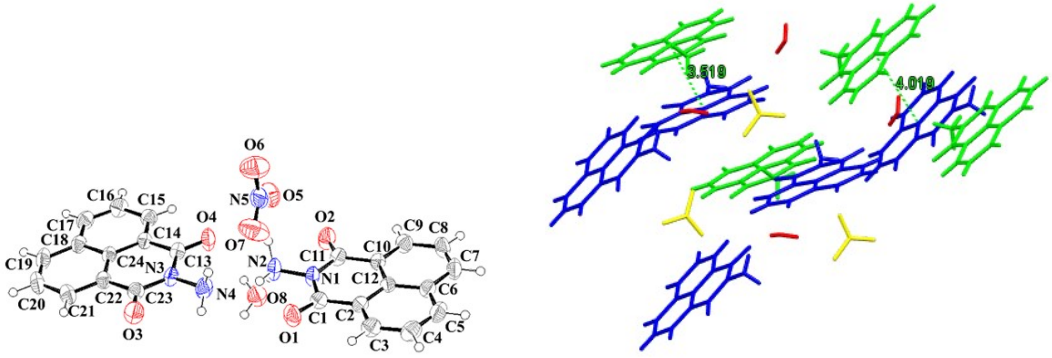

(a) (b)

Figure S7: (a) Structure of the **[HL]NO_3.L.H_2O** ionic co-crystal **(**thermal ellipsoids are with 50% probability) (b) Packing showing the π-stacks among the cations and neutral **L**.

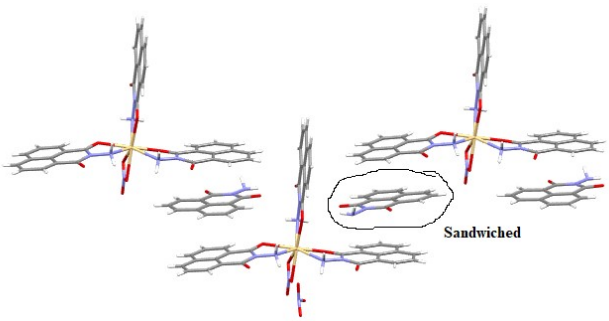

Figure S8: Packing of the **[Cd(L)$_3$(NO_3)] (NO_3).2L** showing the sandwiched L in the self-assembly. **(**thermal ellipsoids are with 50% probability).

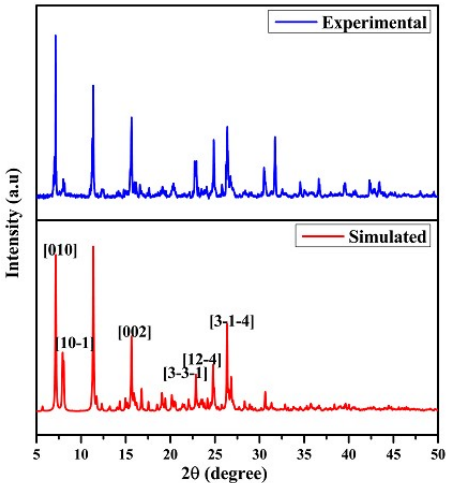

Figure S9: Powder-XRD patterns of the **[Cd(L)$_3$(NO$_3$)] L$_2$(NO$_3$)** complex (top experimental, bottom simulated from CIF file).

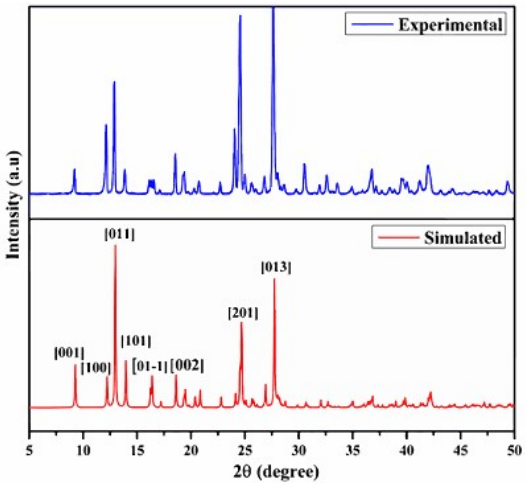

Figure S10: Powder-XRD patterns of the **[CuL$_2$(NO$_3$)$_2$]** complex (top experimental, bottom simulated from CIF file).

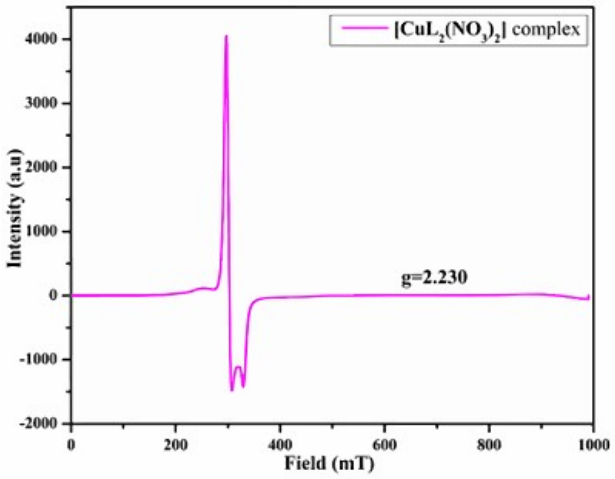

Figure S11: Room temperature X-band ESR spectrum of solid sample of the **$[CuL_2(NO_3)_2]$** complex.

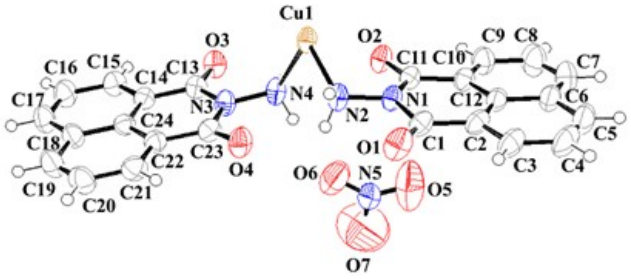

Figure S12: Asymmetric unit of the **$[CuL_4](NO_3)_2$** complex **(**thermal ellipsoids are with 50% probability).

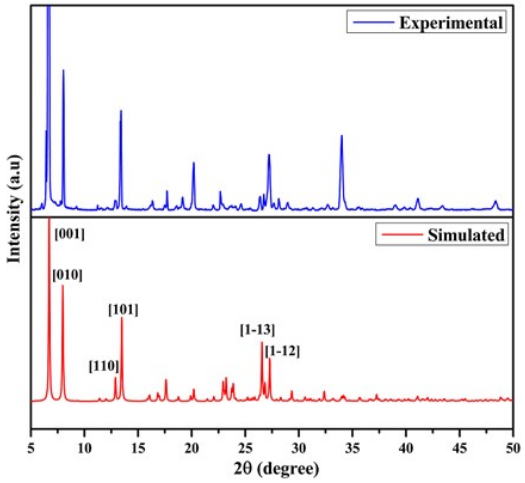

Figure S13: Powder XRDs of **$[CuL_4](NO_3)_2$** complex(top experimental, bottom simulated from CIF file).

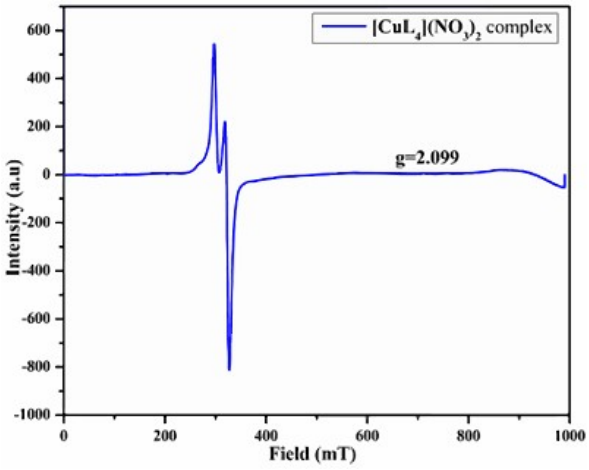

Figure S14: Room temperature X-band ESR spectra of the **$[CuL_4](NO_3)_2$** complex.

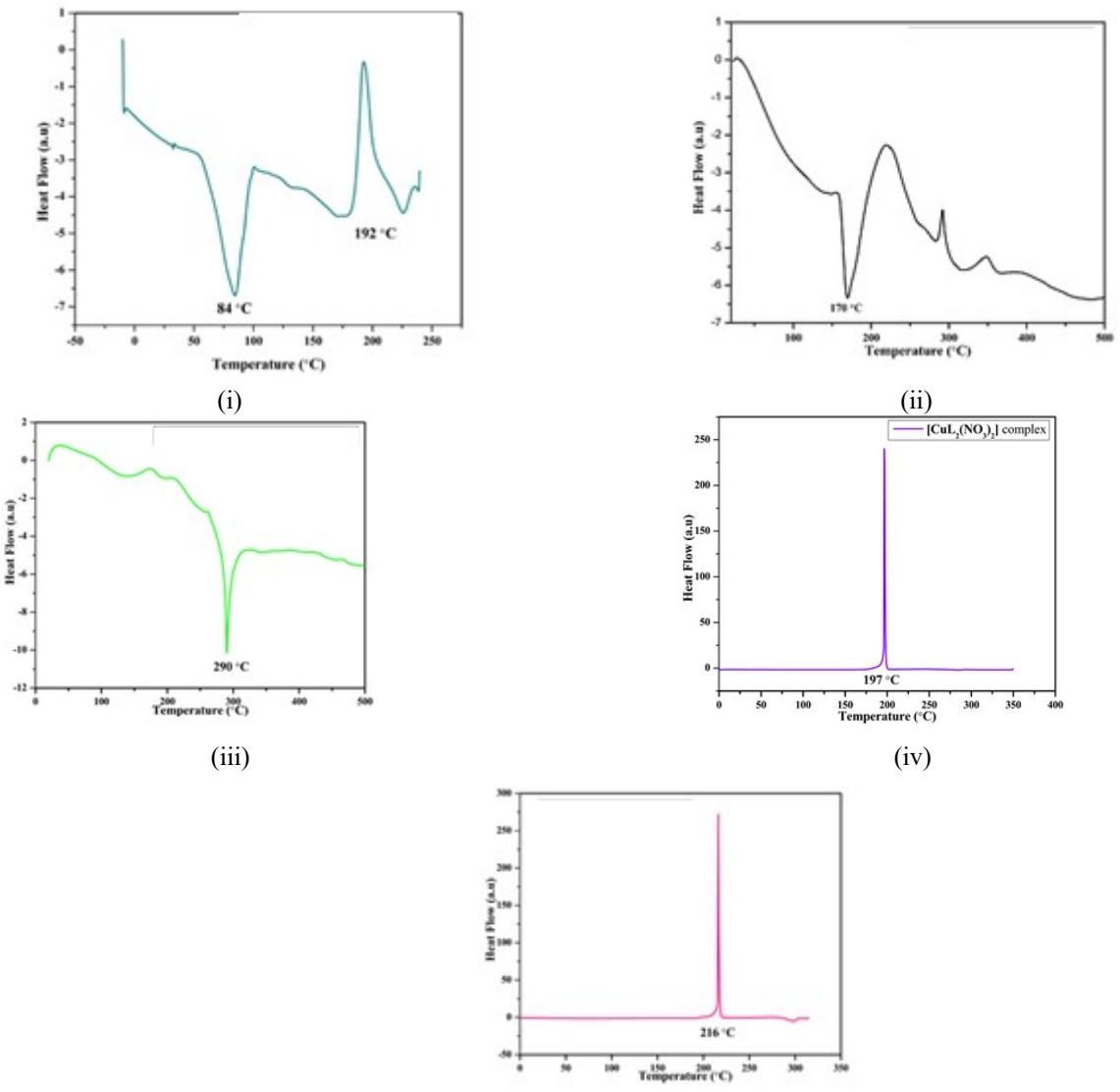

Figure S15: Differential scanning calorimetry plots of the (i) **$[HL]NO_3.H_2O$** salt; (ii) **$[HL]NO_3.L.H_2O$**; (iii) **$[Cd(L)_3(NO_3)](NO_3)2L$** complex; (iv) **$[CuL_2(NO_3)_2]$** complex and (v) **$[CuL_4](NO_3)_2$** complex. (Heating rate 10°C/min under nitrogen atmosphere.

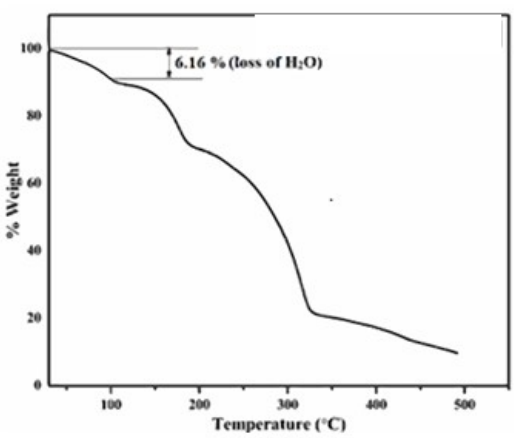

(i)

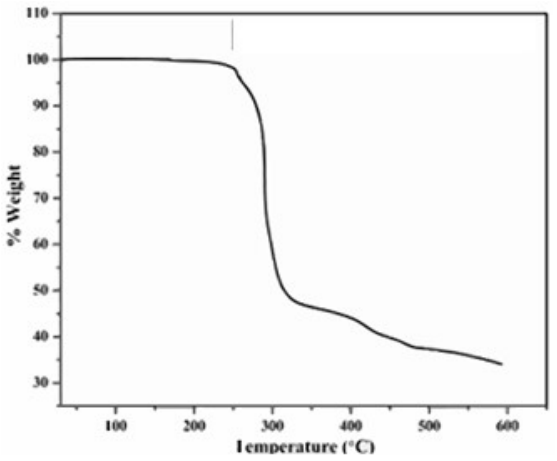

(ii)

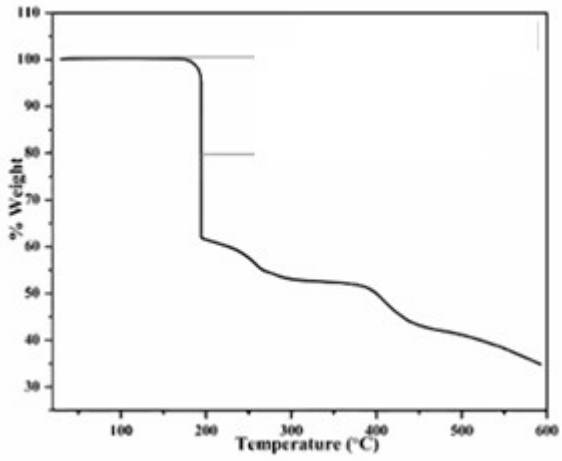

(iii)

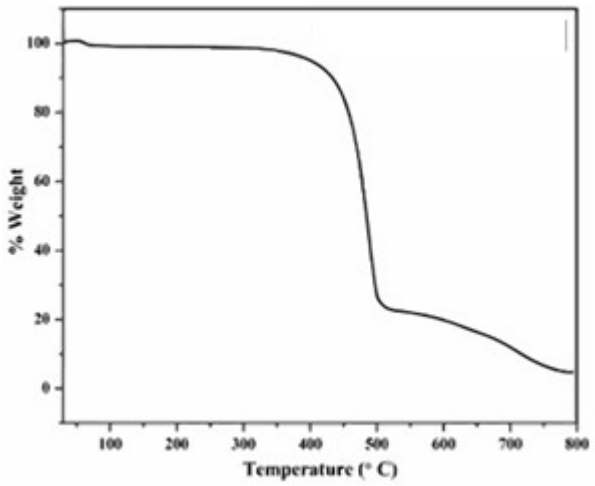

(iv)

Figure S16: Thermogram of the (a) **[HL]NO_3.H_2O** co-crystal; (b) **[$CdL_3(NO_3)$](NO_3).2L** complex; (c) **[CuL_4](NO_3)$_2$** and (d) **[$CuL_2(NO_3)_2$]** complex (heating rate at 10 °C/min under nitrogen atmosphere).

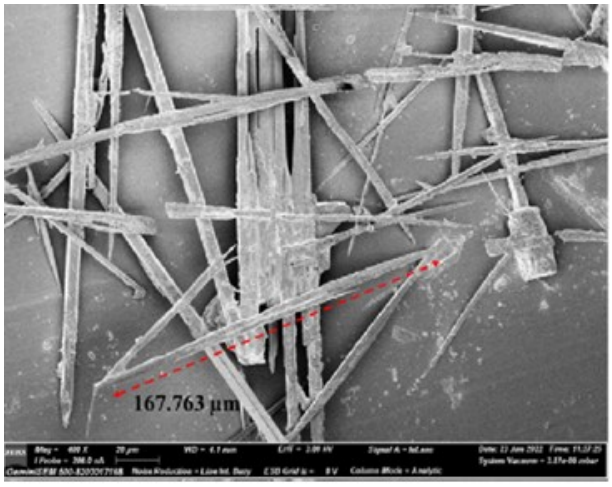

(i)

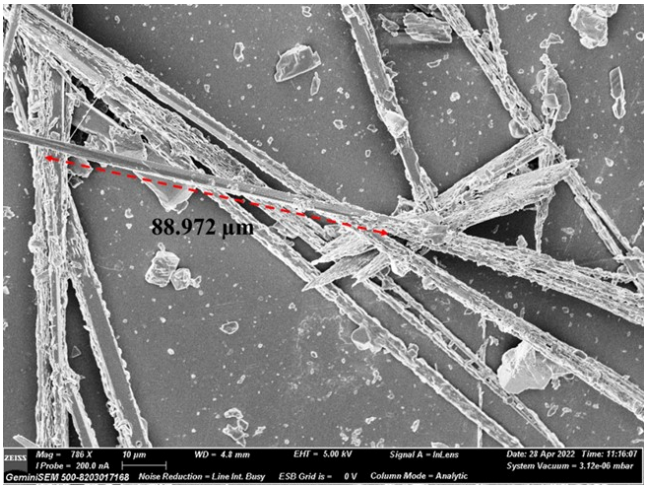

(ii)

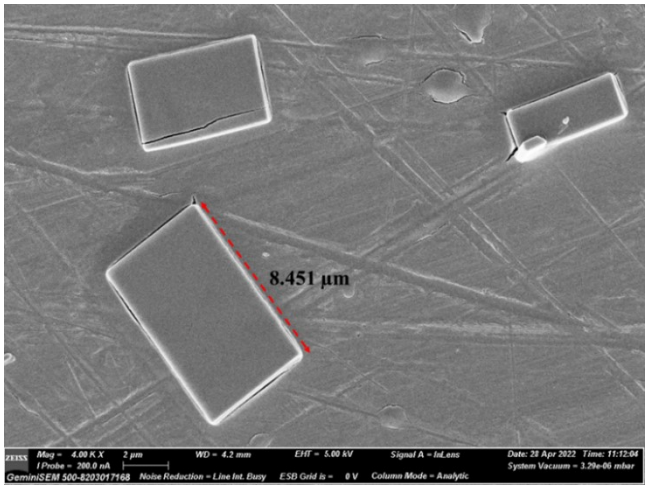

(iii)

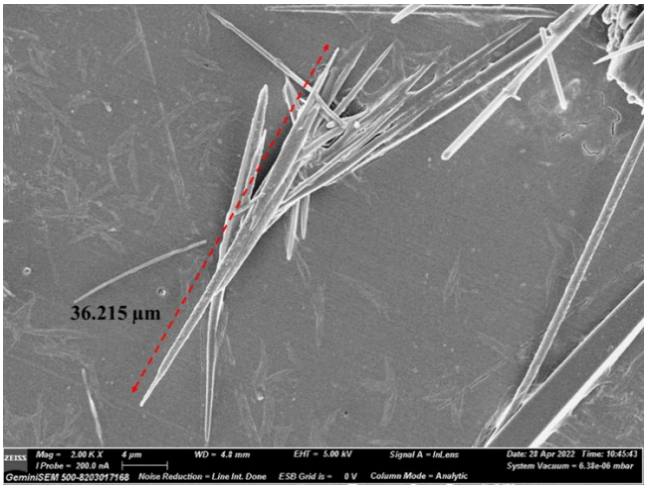

(iv)

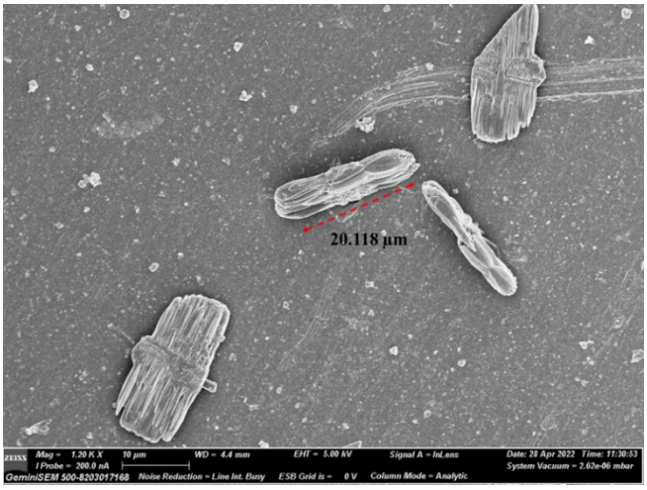

(v)

Figure S17: SEM images of (i) **L-1** (ii) **L-2** (iii) **[HL]NO_3.H_2O**; (iv) **[HL]NO_3.L.H_2O**; (v) **[$CdL_3(NO_3)$](NO_3).2L** complex.

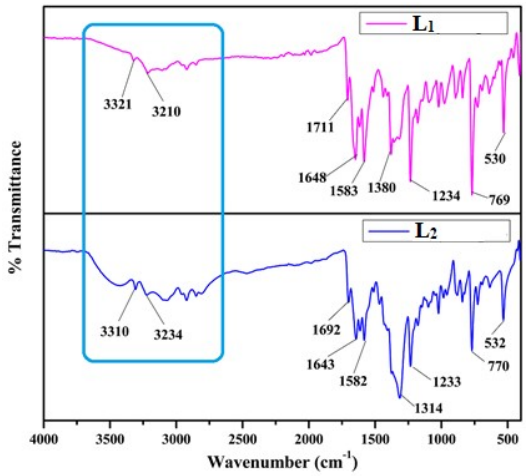

Figure S18: FT-IR spectra of the **L-1** (top) and **L-2** (bottom).

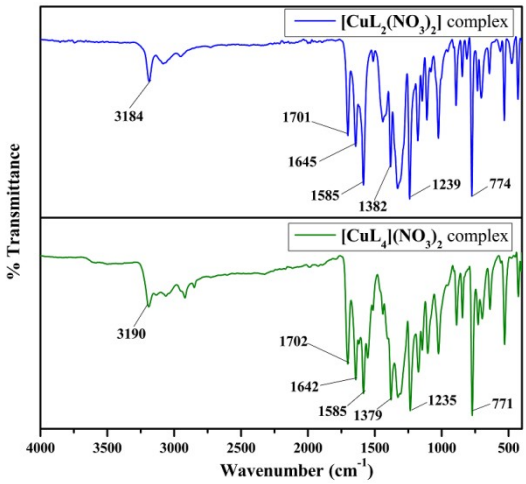

Figure S19: FT-IR spectra of the **$[CuL_2(NO_3)_2]$** (top) and **$[CuL_4](NO_3)_2$** (bottom) complex.

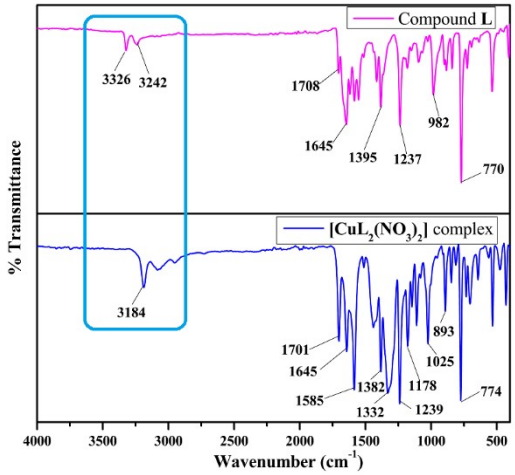

Figure S20**:** FT-IR spectra of the compound **L** and the **$[CuL_2(NO_3)_2]$** complex**.**

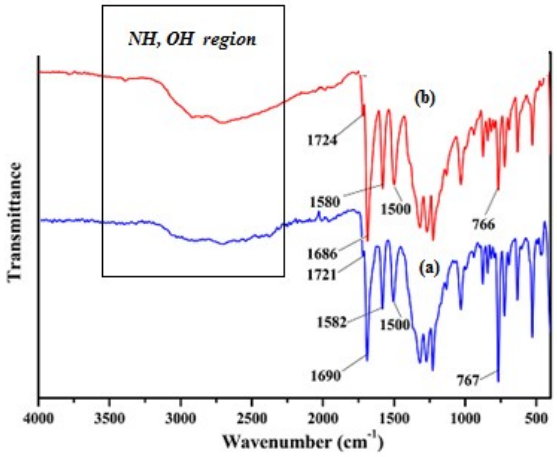

Figure S21: FT-IR spectra of (a) **[HL]NO_3.L.H_2O** and (b) salt **[HL]NO_3.H_2O**.

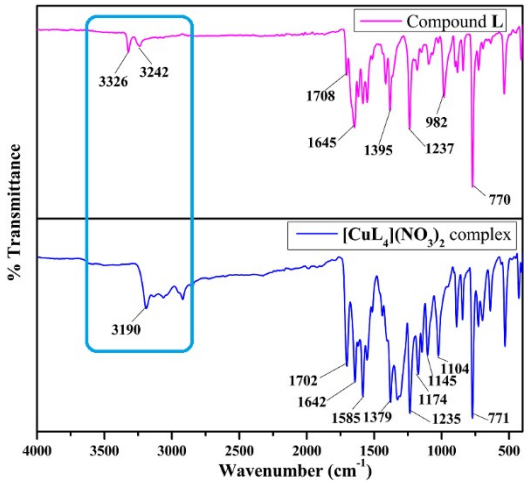

Figure S22: FT-IR spectra of the compound **L** (top) and **[CuL_4](NO_3)$_2$** (bottom)complex**.**

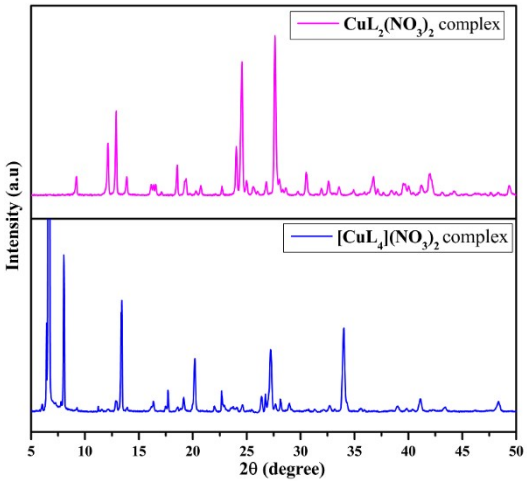

Figure S23: Experimental powder XRD patterns of the **[CuL_2(NO_3)$_2$]** (top) and **[CuL_4](NO_3)$_2$** (bottom) comple

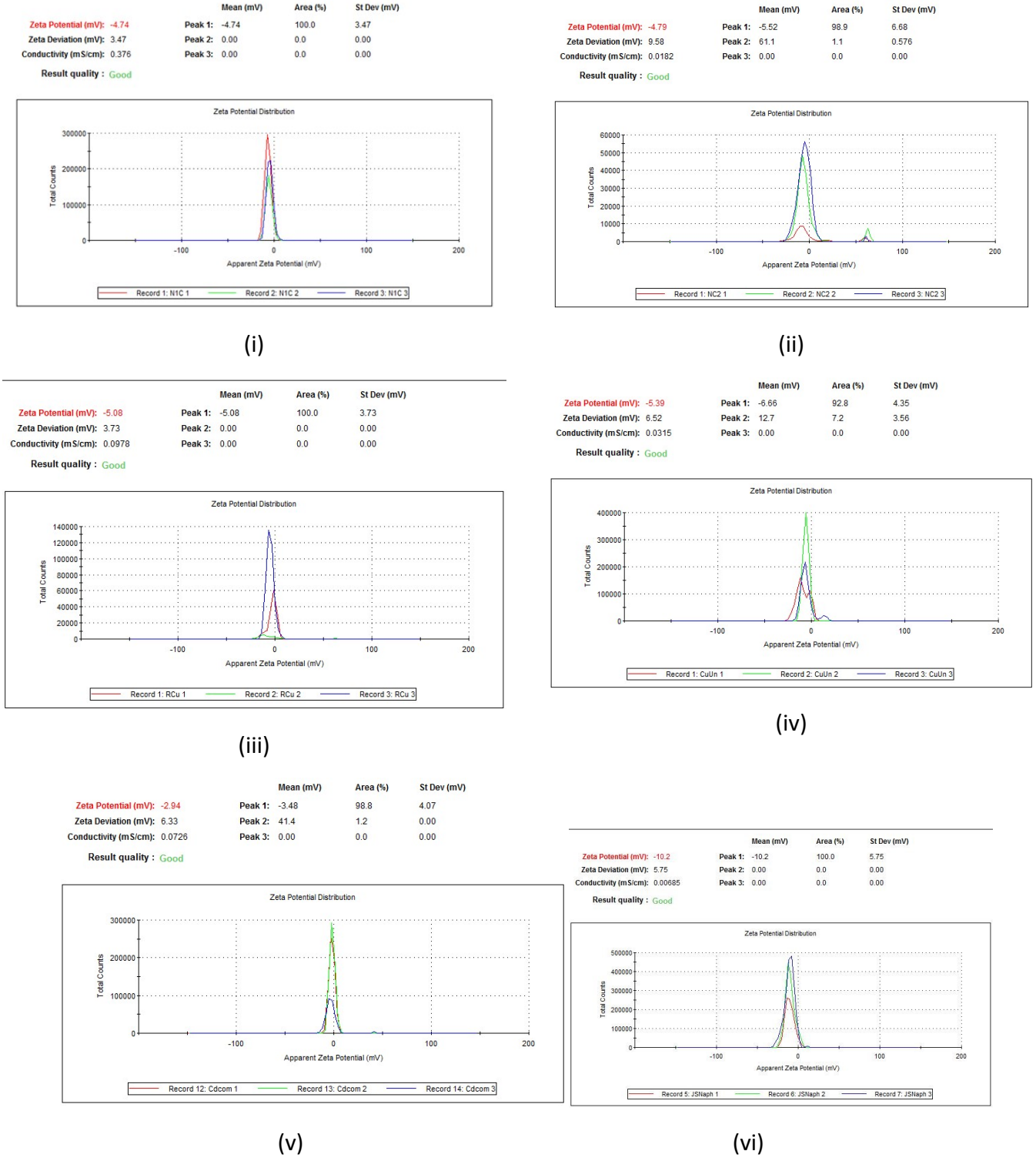

Figure S24: Zeta-potential plots of aqueous solution of (i) **[HL]NO_3.H_2O** (1360 µM) salt; (ii) **[HL]NO_3.L.H_2O** (330 µM) ionic co-crystal; (iii) **[$CuL_2(NO_3)_2$]** (540 µM) complex; (iv) **[CuL_4]$(NO_3)_2$** (225 µM) complex and (v) **[$CdL_3(NO_3)$](NO_3).2L** (257 µM) complex. (vi) **L** (1 mM aqueous solution). In each case 0.5 ml were taken for the respective measurement.

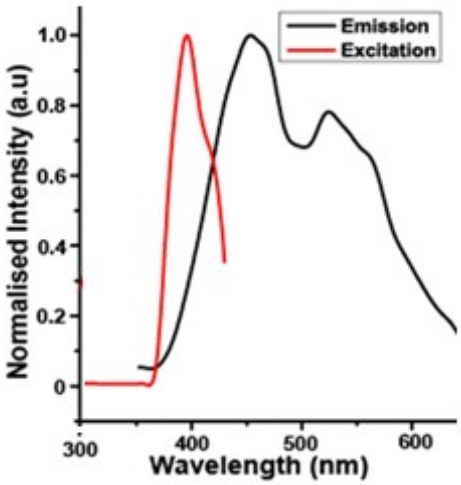

(a)

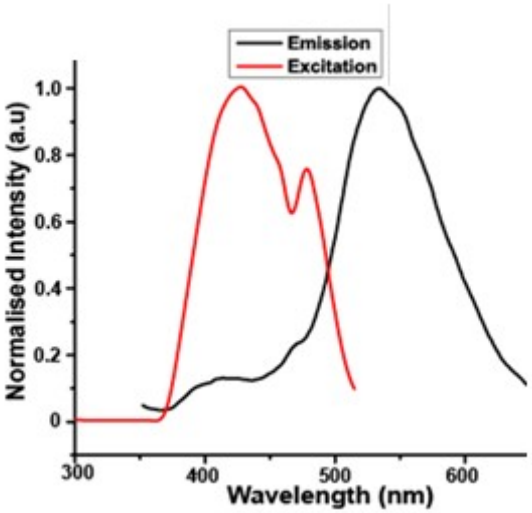

(d)

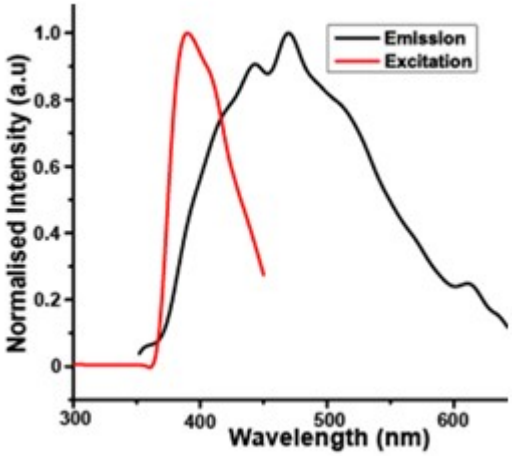

(b)

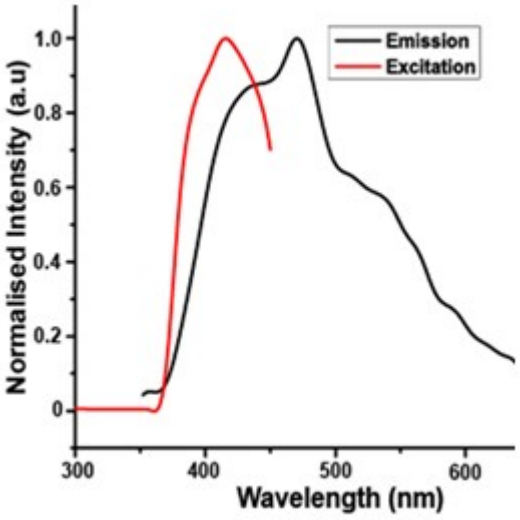

(c)

Figure S25: The excitation and emission spectra of (a) **L**; (b) [**LH**]$NO_3.H_2O$; (c) [**LH**]$NO_3.L.H_2O$; (d) $CdL_3(NO_3)](NO_3).2L$ (in each case 3 ml solution of 10 mM conc. In methanol, λex = 388 in each case).

Table 1S: Hydrogen bond parameters of polymorph, ionic-crystal and metal complexes.

Compound	H-bond	d_{D-H} (Å)	$d_{H...A}$ (Å)	$d_{D...A}$ (Å)	∠DHA (º)
L-2	N(2)-H(2A)···O(1) [1-x, 3-y,- z]	0.86(3)	2.31(3)	3.073(3)	148(2)
	N(2)-H(2B) ···O(3) [x,1+y, z]	1.00(4)	2.35(4)	3.183 (3)	141(3)
	N(4) -H(4A) ···O(2)[x,-1+y,z]	0.89(3)	2.27(3)	3.144(3)	165(2)
	N(4)-H(4B)···O(4) [1-x, -y, 1-z]	0.90(3)	2.21(3)	3.038(3)	154(2)
$[HL]NO_3.H_2O$	N(2)-H(2B) ···O(6) [x, y, 1+z]	0.86	1.83	2.691(3)	171
	N(2)-H(2C) ···O(5) [x, y, 1+z]	0.99	1.76	2.745(3)	174
	O(6)-H(6A) ···O(3) [x, y, z]	0.85	2.47	3.159(3)	139
	O(6)-H(6A) ···O(5) [x, y, z]	0.85	2.04	2.867(3)	164
	O(6)-H(6B) ···O(2) [-x 1-y, 1-z.]	0.85	2.12	2.957(3)	171
$[HL]NO_3L_.H_2O$	N(2)-H(2A) ···O(8) [-1+x, y, -1+z]	0.87	1.86	2.726(4)	175
	N(2)-H(2B) ···N(5) [x, y, -1+z]	0.87	2.12	2.890(3)	148
	N(2)-H(2C) ···O(4) [1-x, ½+y, -z]	1.04(5)	1.93(5)	2.847(5)	147(4)
	O(8)-H(8A) ···O(7) [1-x, -1/2+y, 1-z]	0.85	2.00	2.836(4)	166
	O(8)-H(8B) ···O(4) [1-x, ½+y, 1-z]	0.85	2.13	2.915(4)	153
	O(8)-H(8B) ···O(5) [1-x, ½+y, 1-z]	0.85	2.32	3.056(5)	145
$[CuL_4](NO_3)_2$	N(2)-H(2A) ···O(4) [1+x, y, z]	0.89	2.40	3.050(4)	130
	N(2)-H(2B) ···O(5) [1-x, 1-y, 1-z]	0.89	1.99	2.873(5)	171
	N(4)-H(4A) ···O(1) [-1+x, y, z]	0.89	2.10	2.994(4)	176
	N(4)-H(4B) ···O(5) [1-x, 1-y, 1-z]	0.89	2.20	2.935(6)	139